Vanadium thiocarboxylate Metal-Organic Frameworks as efficient photocatalysts for photooxidative desulfurization.

Pablo Salcedo-Abraira*[1,2], Yolanda Pérez*[3,4], Clara García-Abad[3], Nathalie Guillou[5], Patricia Horcajada,[3] Thomas Devic*[2]

[1] Department of Inorganic Chemistry, University of Granada, Avda. Fuente nueva s/n, 18071 Granada, Spain. E-mail: psalcedo@ugr.es

[2] Nantes Université, CNRS, Institut des Matériaux de Nantes Jean Rouxel, IMN, F-44000 Nantes, France. E-mail: thomas.devic@cnrs-imn.fr

[3] IMDEA Energy Institute, Advanced Porous Materials Unit (APMU), Avda. Ramón de la Sagra 3, E-28935 Móstoles, Madrid, Spain E-mail: yolanda.cortes@urjc.es

[4] COMET-NANO group, Departamento de Biología y Geología, Física y Química Inorgánica, ESCET, Universidad Rey Juan Carlos, C/ Tulipán s/n, 28933, Móstoles, Madrid, Spain

[5]Institut Lavoisier de Versailles, UMR CNRS 8180, Université de Versailles St-Quentin en Yvelines, Université Paris Saclay, 78035 Versailles, France.

SUPPORTING INFORMATION

1. Synthesis

Synthesis of H_4DSBDC:

2,5-disulfhydrylbenzene-1,4-dicarboxylic acid (H_4DSBDC) was synthesized based on the procedure published by Vial et al.[1]

Exploratory synthesis of MOFs

Table S1: Summary of the synthesis parameters explored in the system V-H_4DSBDC.

L/M	[V] (M)	LiOH	NaOH	KOH	Solvent	Phase	Crystallinity
1	0.05	2 eq			DMF	Amorphous	-
1	0.05		2 eq		DMF	Amorphous	-
1	0.05			2 eq	DMF	(DMA)KVO(DSBDC)	Good
1	0.05			4 eq	DMF	Amorphous	-
1	0.05			6 eq	DMF	Amorphous	
1	0.05			2 eq	DMF:MeOH 8:2	Amorphous	-
1	0.05				DMF:MeOH 8:2	MIL-47(V)-$(SCH_3)_2$	Low, impurities
1.5	0.05				DMF:MeOH 8:2	MIL-47(V)-$(SCH_3)_2$	Good
1.5	0.05				DMF:MeOH	MIL-47(V)-$(SCH_3)_2$	Low

					9:1		
1.5	0.05				DMF:MeOH 6:4	MIL-47(V)-$(SCH_3)_2$	Low
1.5	0.05				DMF:MeOH 5:5	MIL-47(V)-$(SCH_3)_2$	Low
1.5	0.05				DMF	Amorphous	-
1.5	0.05				DMF:EtOH 8:2	Unknown phase	-
1.5	0.05				DMF:iPrOH 8:2	Amorphous	-

2. Chemical analysis of the MOFs

The chemical composition of each material was corroborated by a combination of elemental analysis (C, H, N, S) and inductively coupled plasma-atomic emission spectroscopy (ICP-AES; K, V), being the oxygen estimated by difference:

(DMA)KVO(DSBDC): Theo. (%): C 31.74; H 2.77; N 3.70; S 16.95; K 10.33; V 13.46; O 21.14. Exp. (%): C 31.1 ± 0.6; H 2.7 ± 0.1; N 3.4 ± 0.1; S 15.6 ± 1.4; K 10.2 ± 0.2; V 13.4 ± 0.2

MIL-47(V)-$(SCH_3)_2 \cdot (H_2O)$: Theo. (%): C 35.09; H 3.23; S 18.73; V 14.88; O 28.04. Exp. (%): C 35.46 ± 0.6; H 3.08 ± 0.05; S 18.5 ± 0.5; V 14.6 ± 0.2

3. Optical and electron microscopy

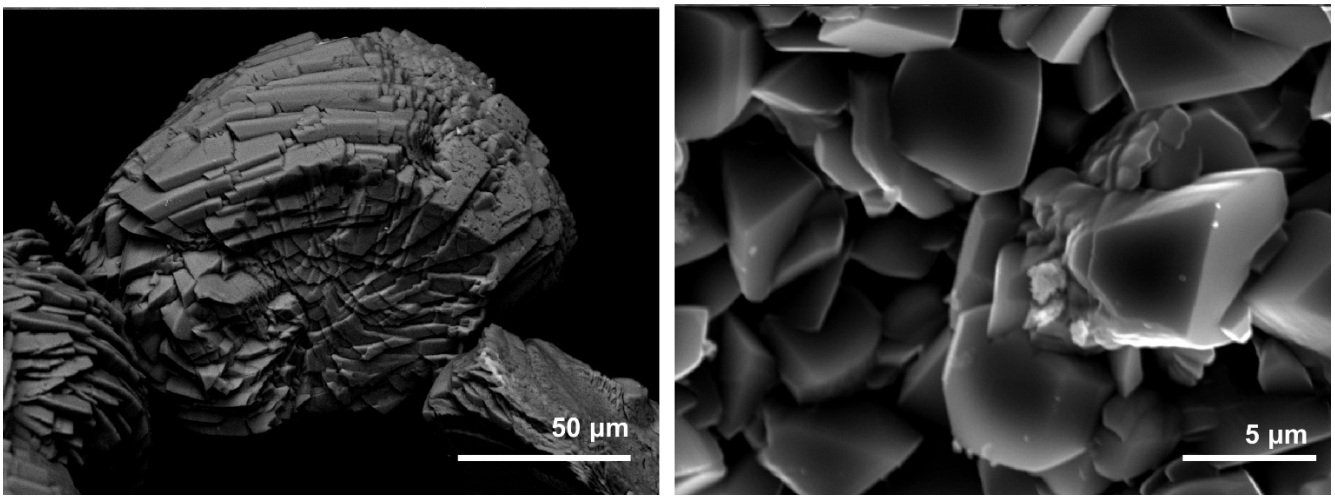

Figure S1: SEM images of (DMA)KVO(DSBDC) materials prepared from VCl_3 (left) and VO(acac) (right).

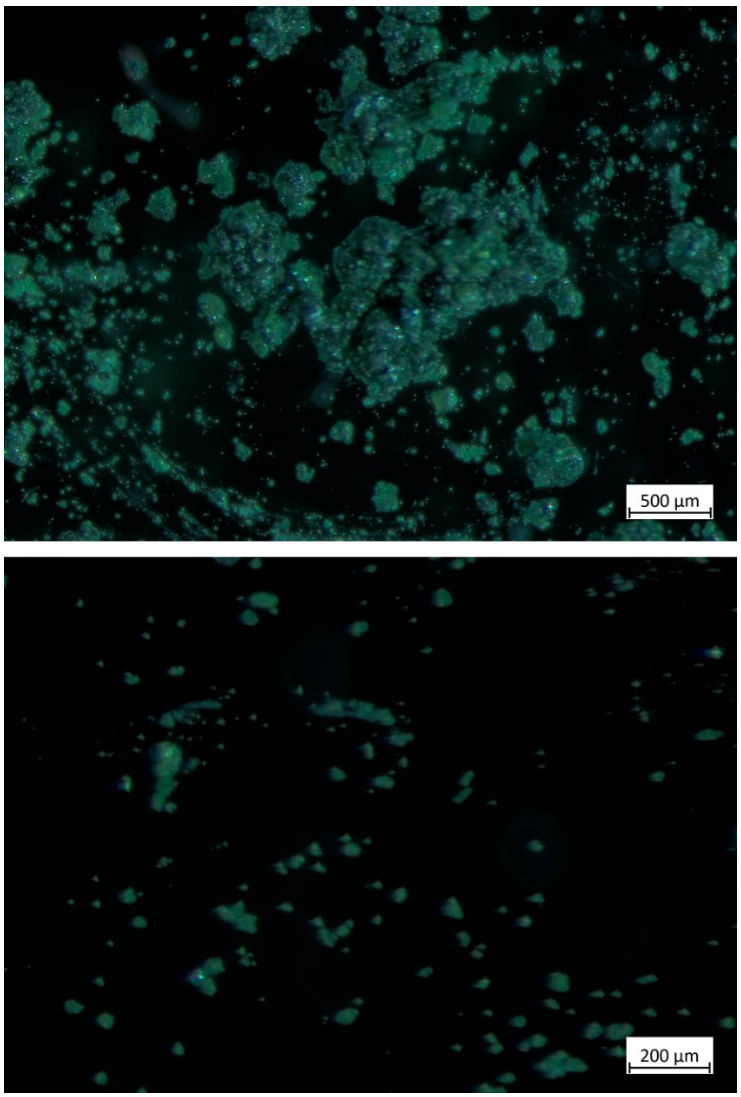

Figure S2: Optical microscope images of (DMA)KVO(DSBDC) synthesized from VCl_3.

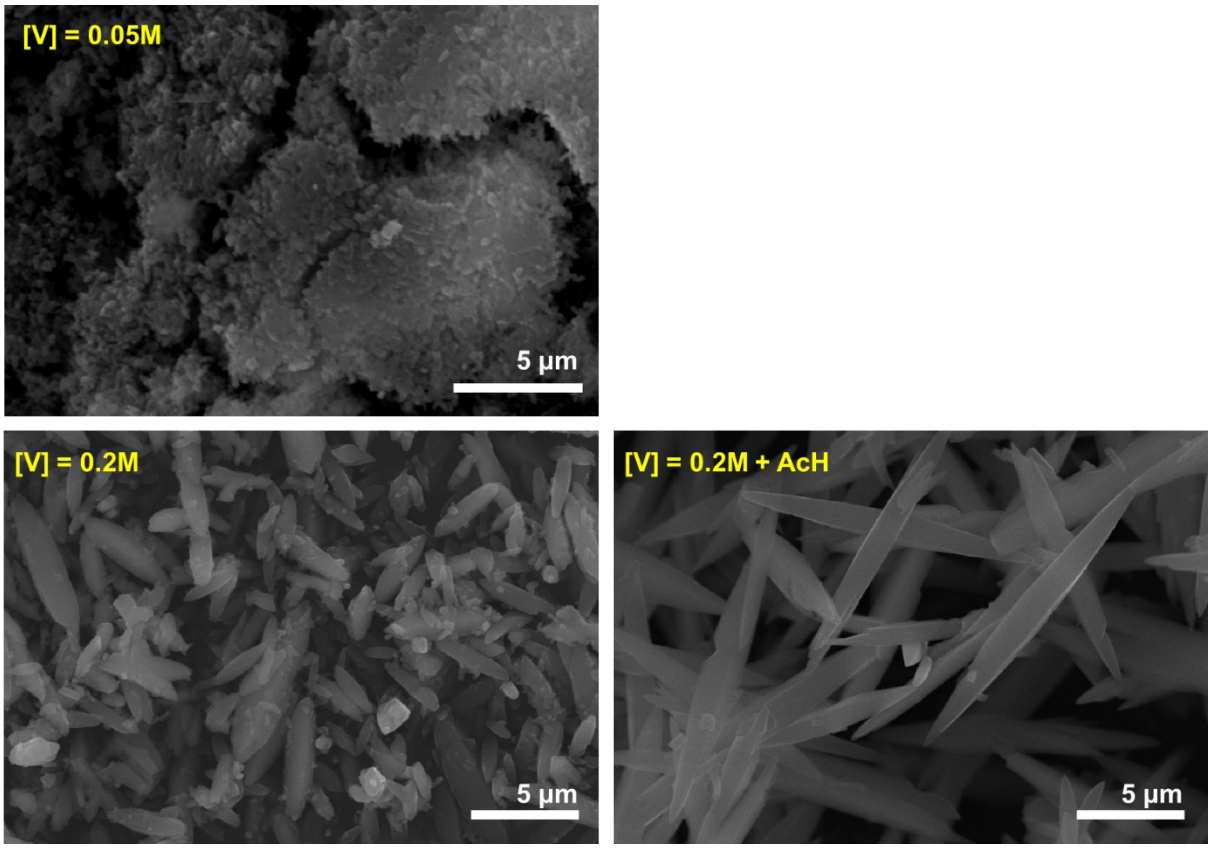

Figure S3: SEM images of MIL-47(V)-$(SCH_3)_2$ without modulator (left) and with acetic acid as modulator (right).

3. Structural characterization

Table S2: Relevant crystallographic information of (DMA)KVO(DSBDC)

Chemical formula	$VC_{10}H_{10}KNO_5S_2$
M_r	378.35
Crystal system, space group	Triclinic, *P*-1
***a*, *b*, *c* (Å)**	6.9416(5), 10.3763(7), 10.4436(7)
α*, *β*, *γ	101.025(6), 101.363(6), 98.543(6)
***V* (Å^3)**	710.19(9)
Z	2
ρ_{calc} **(g cm^{-3})**	1.769
μ_{CuKa} **(mm^{-1})**	1.300
***F*(000)**	382
Crystal size (mm)	0.05x0.04x0.036
T_{min}, T_{max}	1.000, 0.861
Data collection temperature (K)	296.15
Radiation, λ (Å)	MoKa, 0.71073
θ_{min}, θ_{max} (°)	3.254, 30.307
h_{min}, h_{max}	-9, 8
k_{min}, k_{max}	-14, 13
l_{min}, l_{max}	-13, 13
No. of measured, unique and observed [$I \geq 2\sigma(I)$] reflections	3500, 3500, 2142
R_{int}	0.0914
No. of reflections, No. of parameters, no. of Restrains	3500, 189, 0
$R[F^2 > 2\sigma(F^2)]$, $wR(F^2)$, S	0.0490, 0.1223, 0.818
ρ_{min}, ρ_{max} (e Å^{-3})	-0.408, 0.397

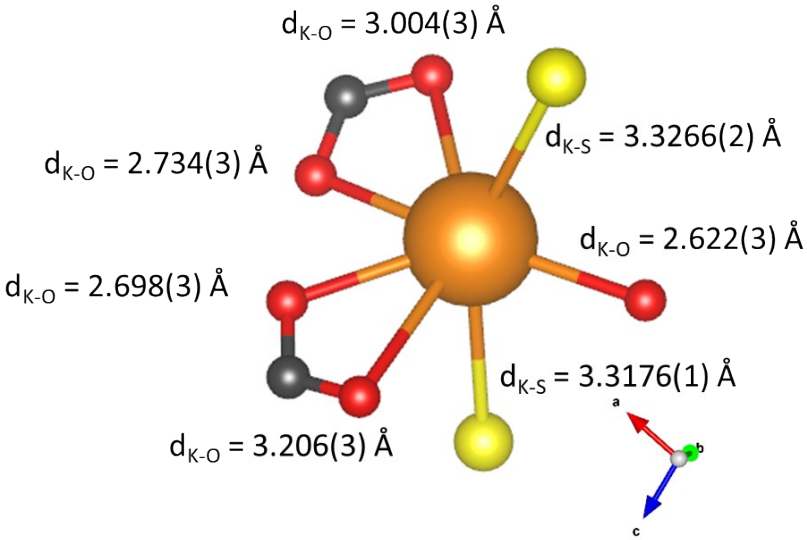

Figure S4: Crystallographic interatomic distances between K^+ ion and the surrounding atoms of (DMA)KVO(DSBDC).

Table S3: Crystallographic information of MIL-47(V)-$(SCH_3)_2$

Compound	$VOH(C_{10}H_8S_2O_4)$
Crystal system	Monoclinic
Wavelength	0.671415 Å
Space group	*C*2/*c*
a	18.9190(4) Å
b	11.6119(3) Å
c	6.87187(2) Å
β	108.9768(1) °
V	1427.60(7) $Å^3$
R_{wp}, R_p	0.0501, 0.0415
R_{Bragg}	0.0398

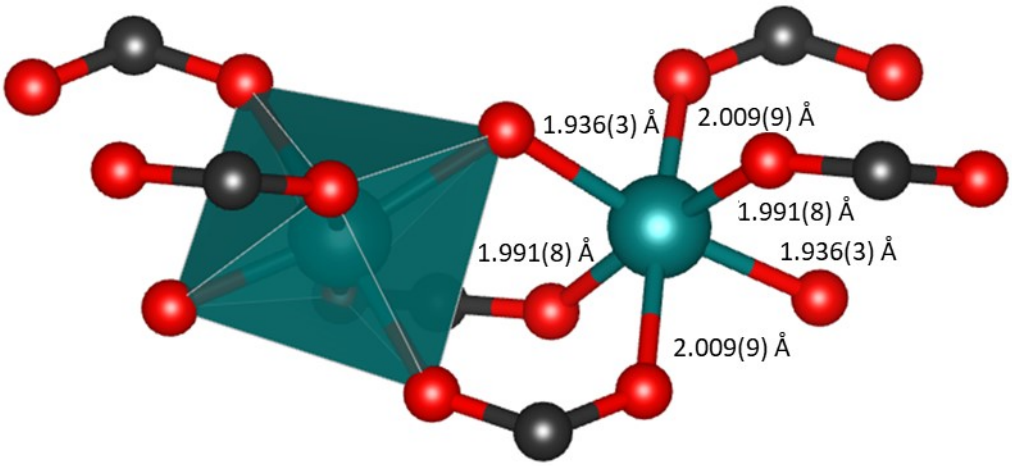

Figure S5: V-O bond distances of MIL-47(V)-$(SCH_3)_2$.

4. Powder X-Ray Diffraction

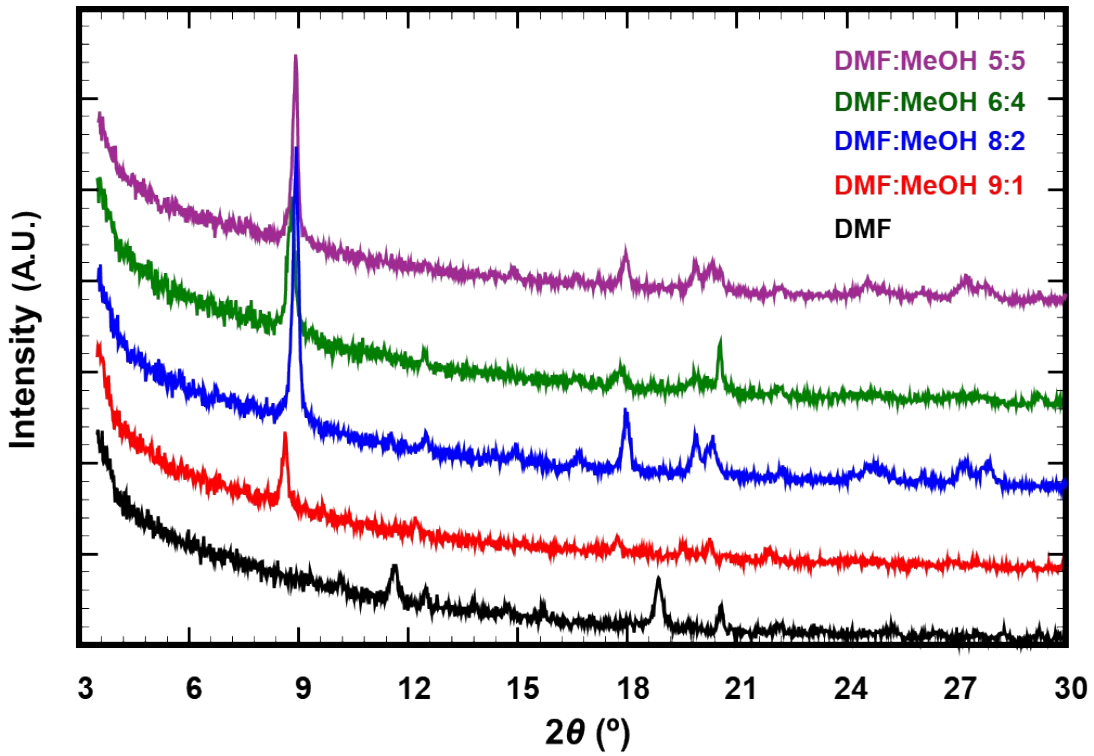

Figure S6: PXRD patters of MIL-47(V)-$(SCH_3)_2$ synthetic screening depending on the solvent mixture used.

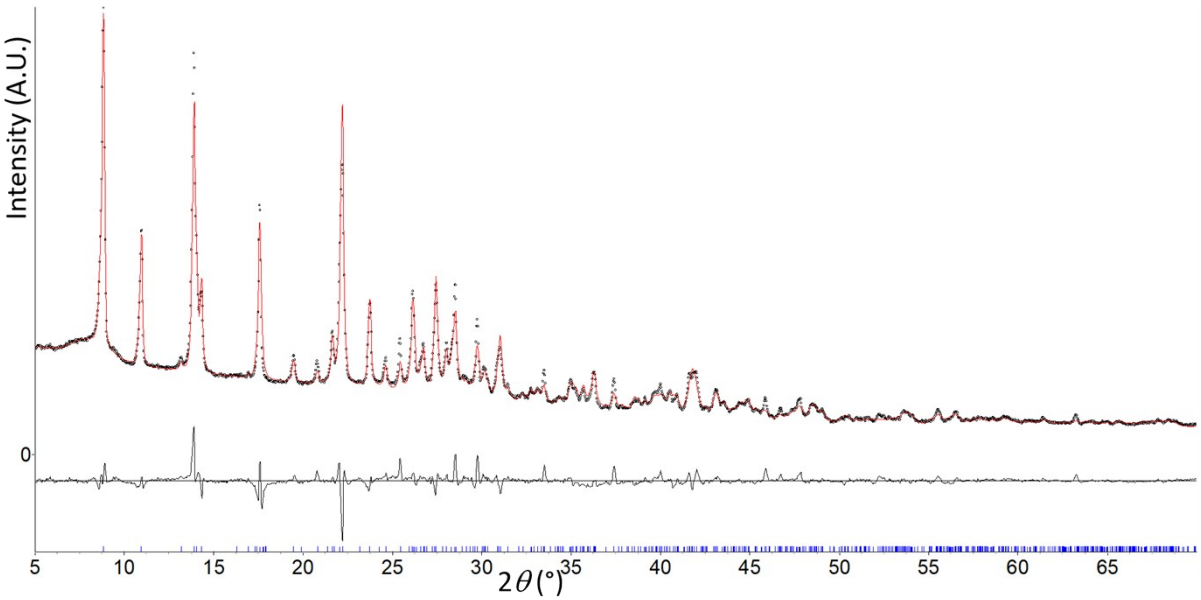

Figure S7: Rietveld plot of (DMA)KVO(DSBDC) material (λ = 1.54059Å, R_{wp} =0.0508 R_{Bragg} = 0.031) showing observed (black dots), calculated (red line) and difference (black line) curves. Only the profile parameters have been refined.

Table S4: Unit cell parameters of (DMA)KVO(DSBDC) obtained by SC-XRD and PXRD, both at room temperature.

	SC-XRD	PXRD
Space group	*P*-1	*P*-1
a	6.9416(5) Å	6.9860(8) Å
b	10.3763(7) Å	10.403(2) Å
c	10.4436(7) Å	10.470(2) Å
α	101.025(6) °	101.149(6) °
β	101.363(6) °	101.532(9) °
γ	98.543(6) °	98.973(8) °
V	710.19(9) Å^3	716.3(2) Å^3

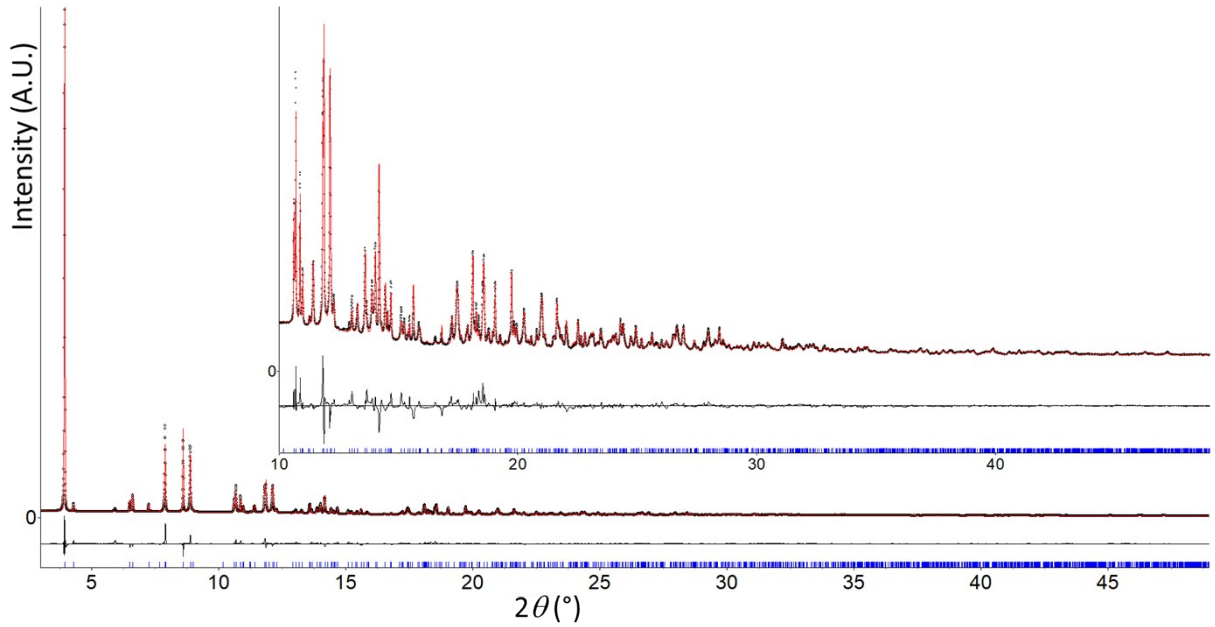

Figure S8: Final Rietveld plot of MIL-47(V)-$(SCH_3)_2$ (λ = 0.671415Å) showing observed (black dots), calculated (red line) and difference (black line) curves. A zoom is shown as inset.

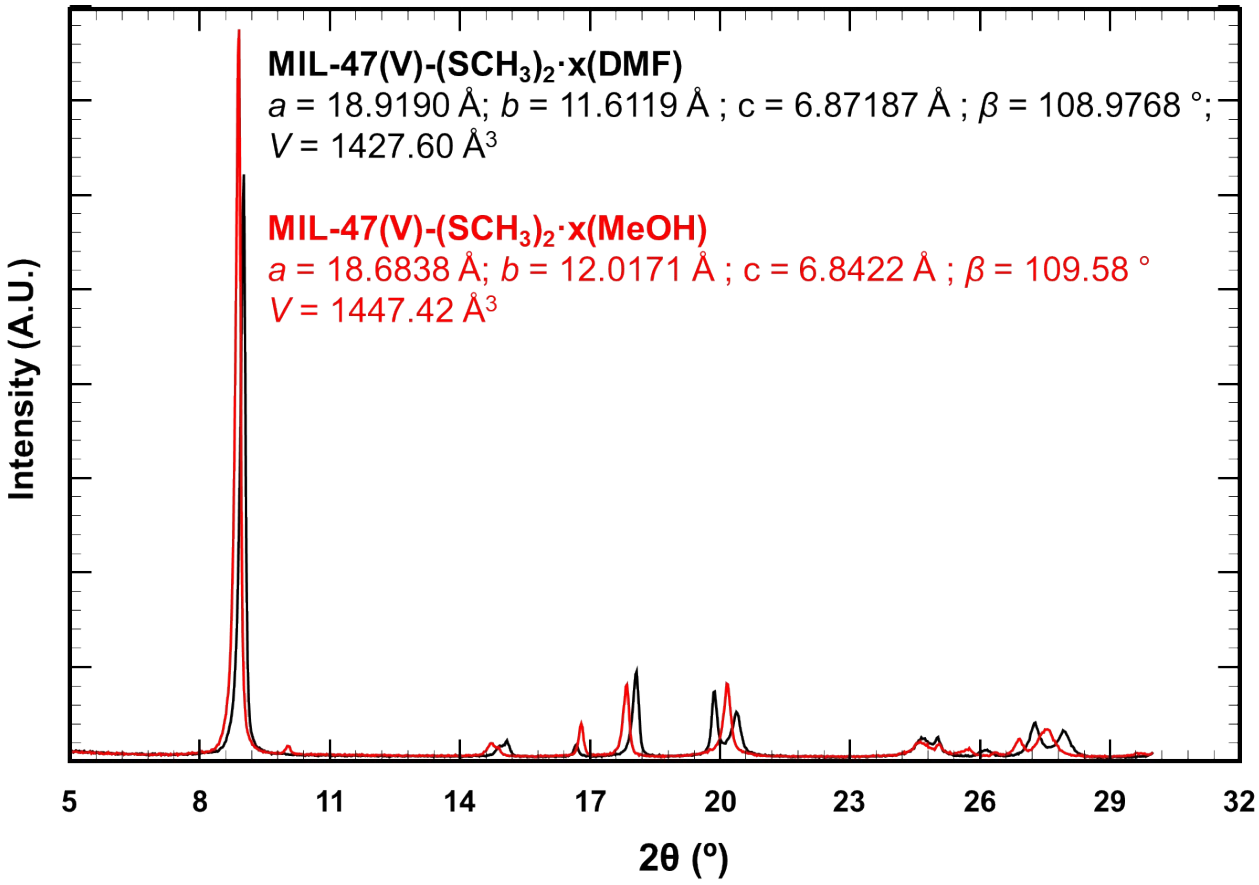

Figure S9: PXRD of the MIL-47(V)-$(SCH_3)_2$ solid before (black) and after (red) solvent exchange in MeOH. The deduced unit-cell parameters are also shown.

5. Textural properties.

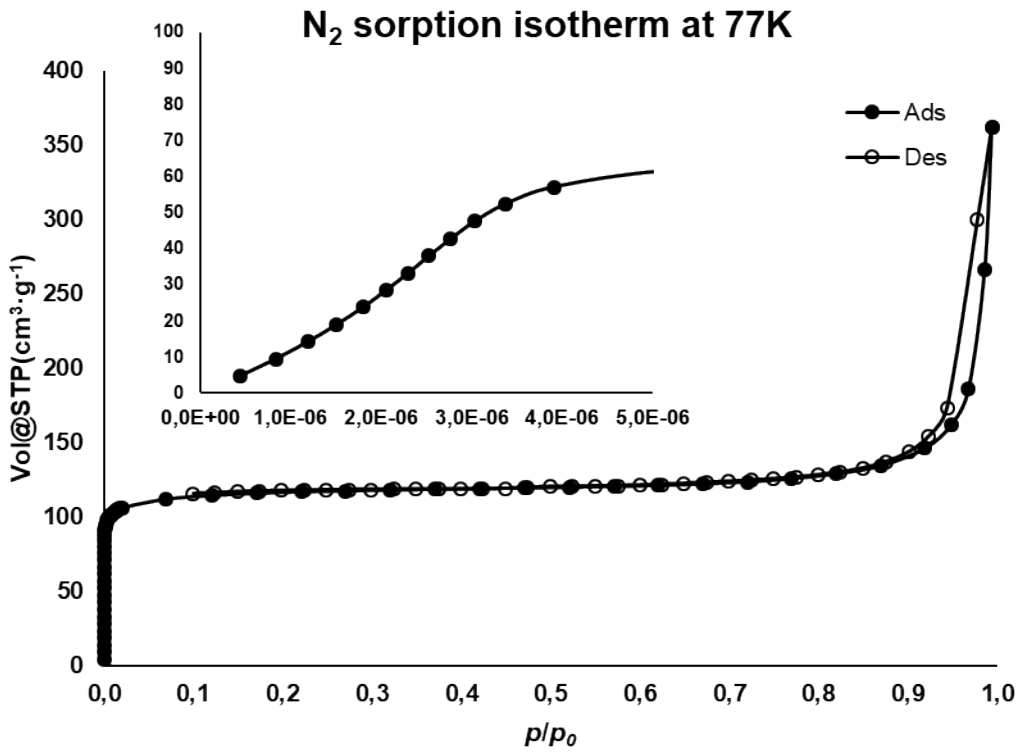

Figure S10: N_2 sorption isotherm of MIL-47(V)-$(SCH_3)_2$ at 77K

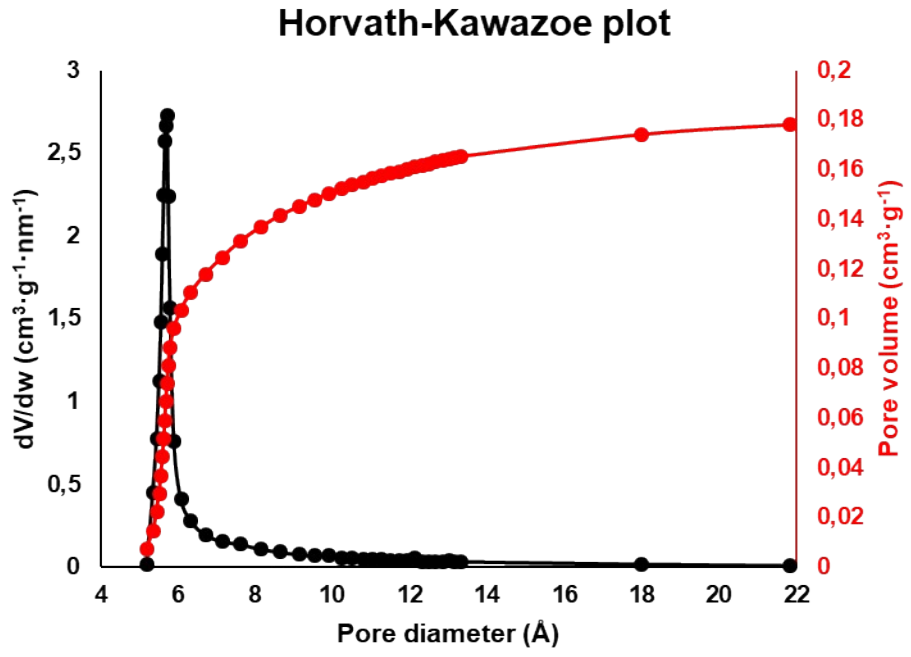

Figure S11: Horvath-Kawazoe pore size distribution of MIL-47(V)-$(SCH_3)_2$

6. Infrared spectroscopy

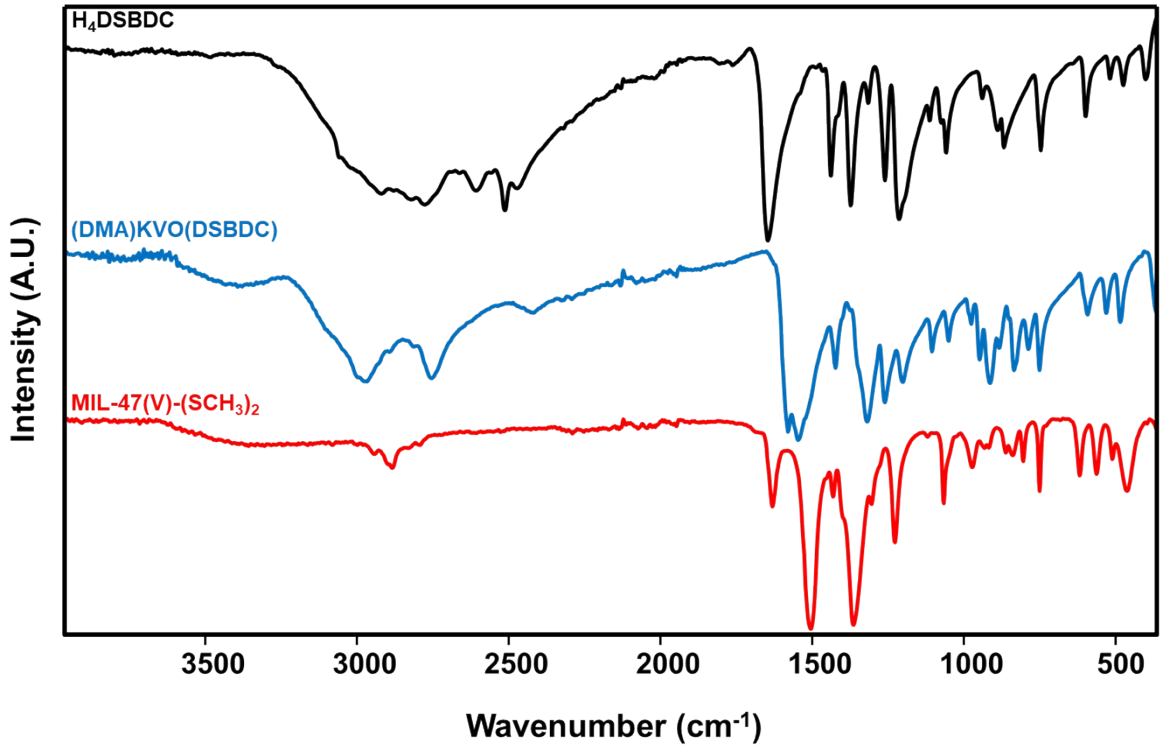

Figure S12: FTIR spectra of H_4DSBDC (black), (DMA)KVO(DSBDC) (blue) and MIL-47(V)-$(SCH_3)_2$·x(DMF)

Table S5: Main vibration bands and their assigned wavenumber of the different functional groups present in DSBDC, (DMA)KVO(DSBDC) and MIL-47-$(SCH_3)_2$.

Band	H_4DSBDC	(DMA)KVO(DSBDC)	MIL-47(V)-$(SCH_3)_2$
ν S-H	2547 cm^{-1}	-	-
ν COO	1680 cm^{-1}	1614, 1581 cm^{-1}	1541 cm^{-1}
ν C-S	634 cm^{-1}	627 cm^{-1}	654, 598 cm^{-1}
ν N-H	-	3011 cm^{-1}	-
ν $C-H_{alifatic}$	-	2852, 2788 cm^{-1}	2981, 2919, 2830 cm^{-1}
ν V=O	-	950 cm^{-1}	-
ν V-O-V	-	-	546 cm^{-1}
γ(OH)			497 cm^{-1}
ν CO-DMF	-	-	1667 cm^{-1}

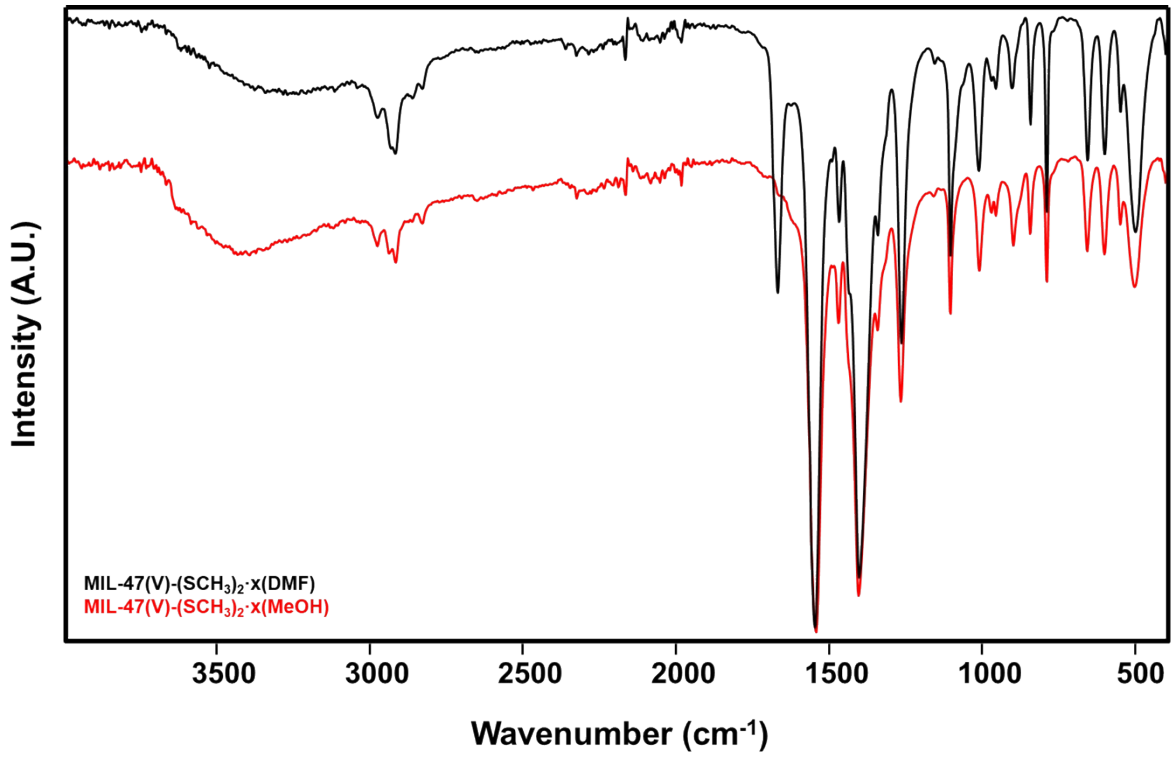

Figure S13: FTIR spectra of the MIL-47(V)-$(SCH_3)_2$ solid before (black) and after (red) solvent exchange in MeOH.

.

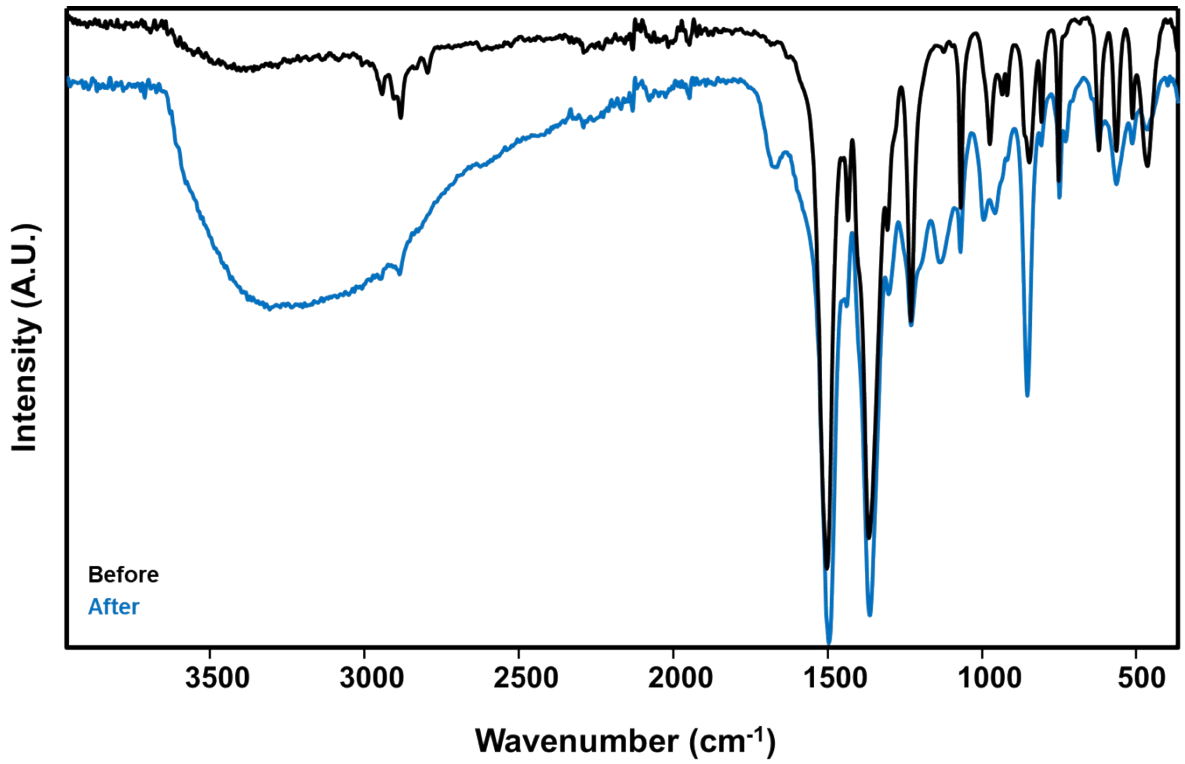

Figure S14: FTIR spectra of MIL-47(V)-$(SCH_3)_2 \cdot x CH_3OH$ thermal reversibility before (black) and after (blue) under air.

7. Thermal stability

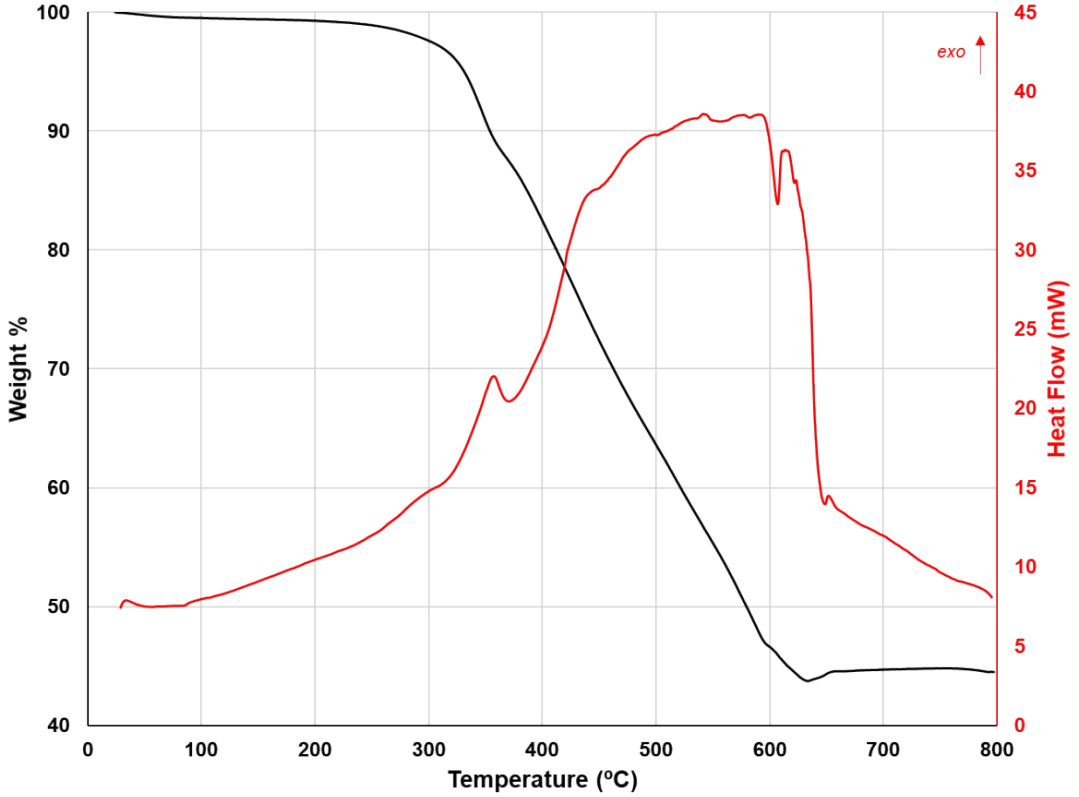

Figure S15: TGA-DSC curve of (DMA)KVO(DSBDC).

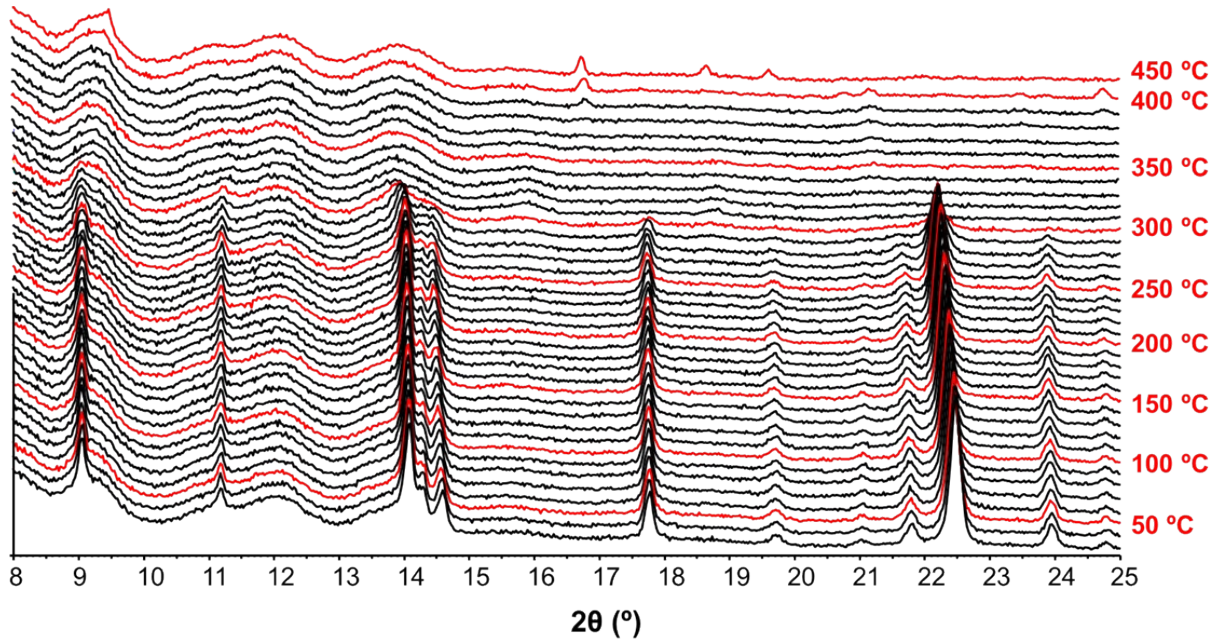

Figure S16: VT-PXRD of (DMA)KVO(DSBDC).

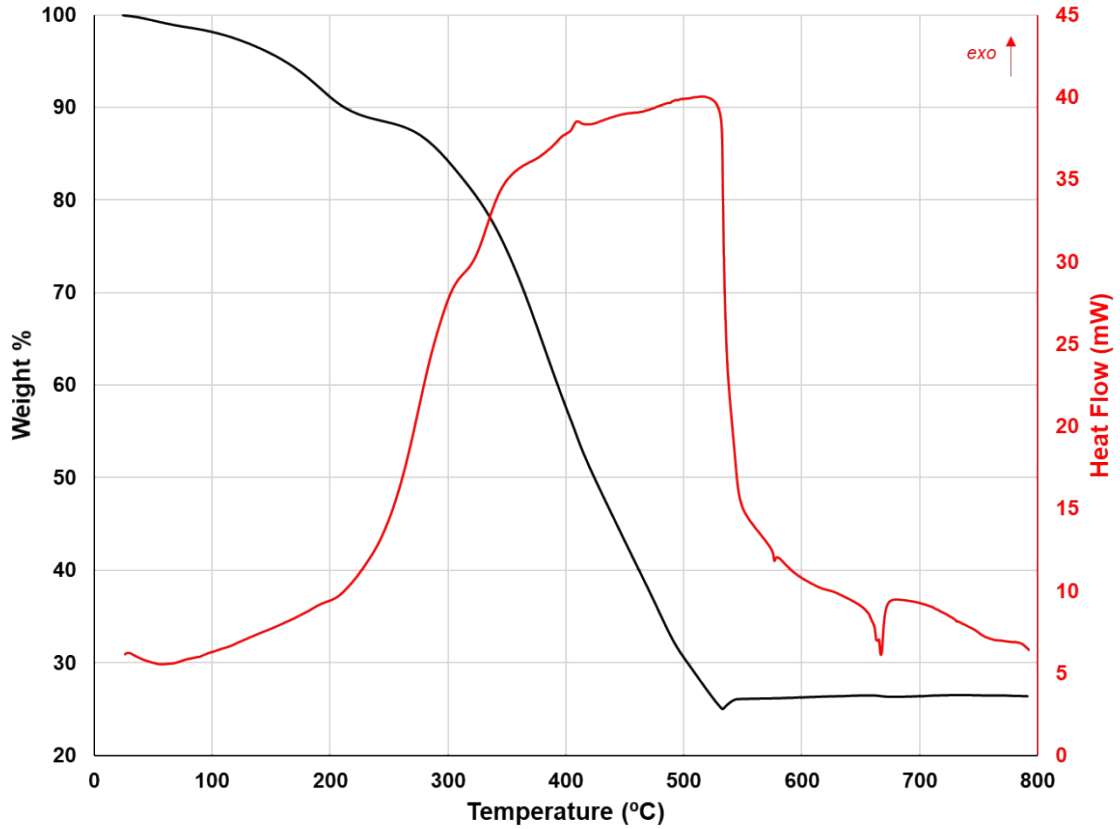

Figure S17: TGA-DSC curve of MIL-47(V)-$(SCH_3)_2 \cdot x$DMF·

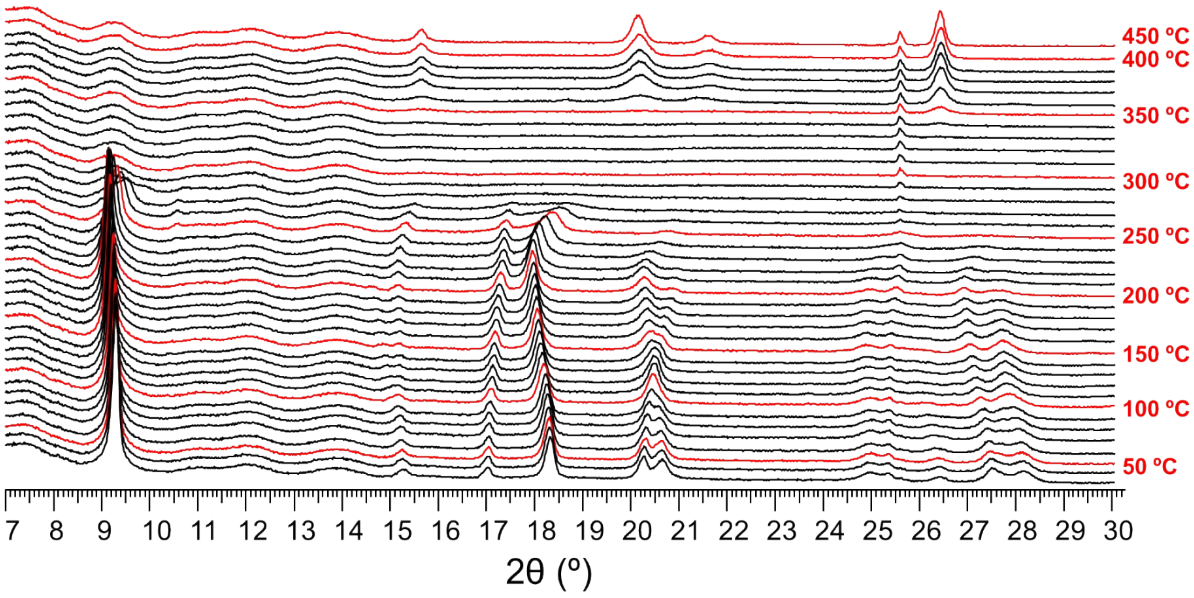

Figure S18: VTPXRD of MIL-47(V)-$(SCH_3)_2 \cdot x$DMF·

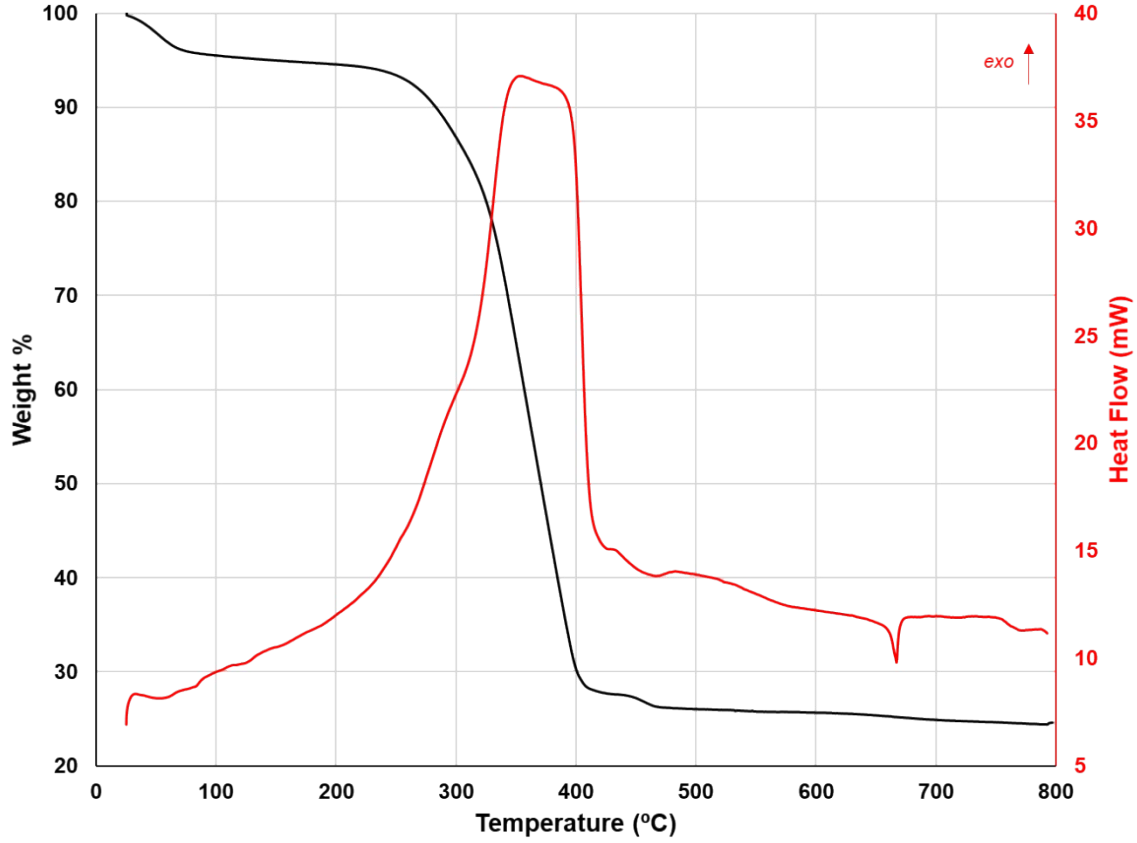

Figure S19: TGA-DSC curve of MIL-47(V)-$(SCH_3)_2 \cdot x CH_3OH$

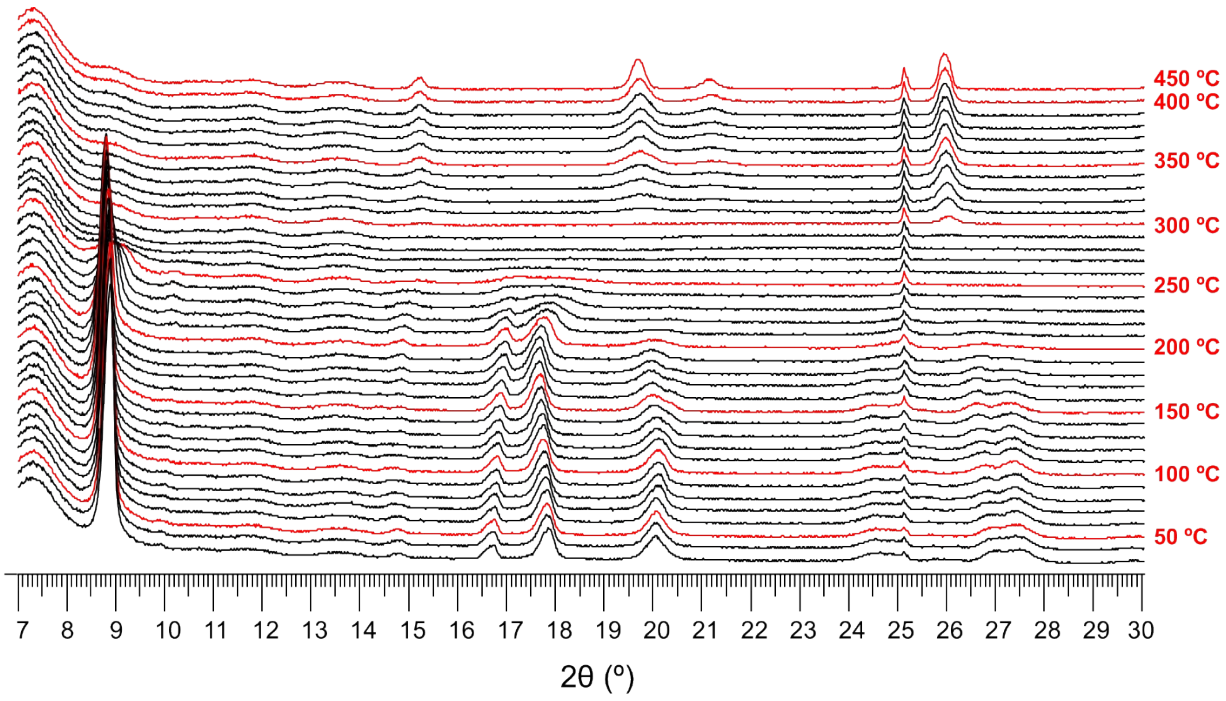

Figure S20: VTPXRD of MIL-47(V)-$(SCH_3)_2 \cdot x CH_3OH$

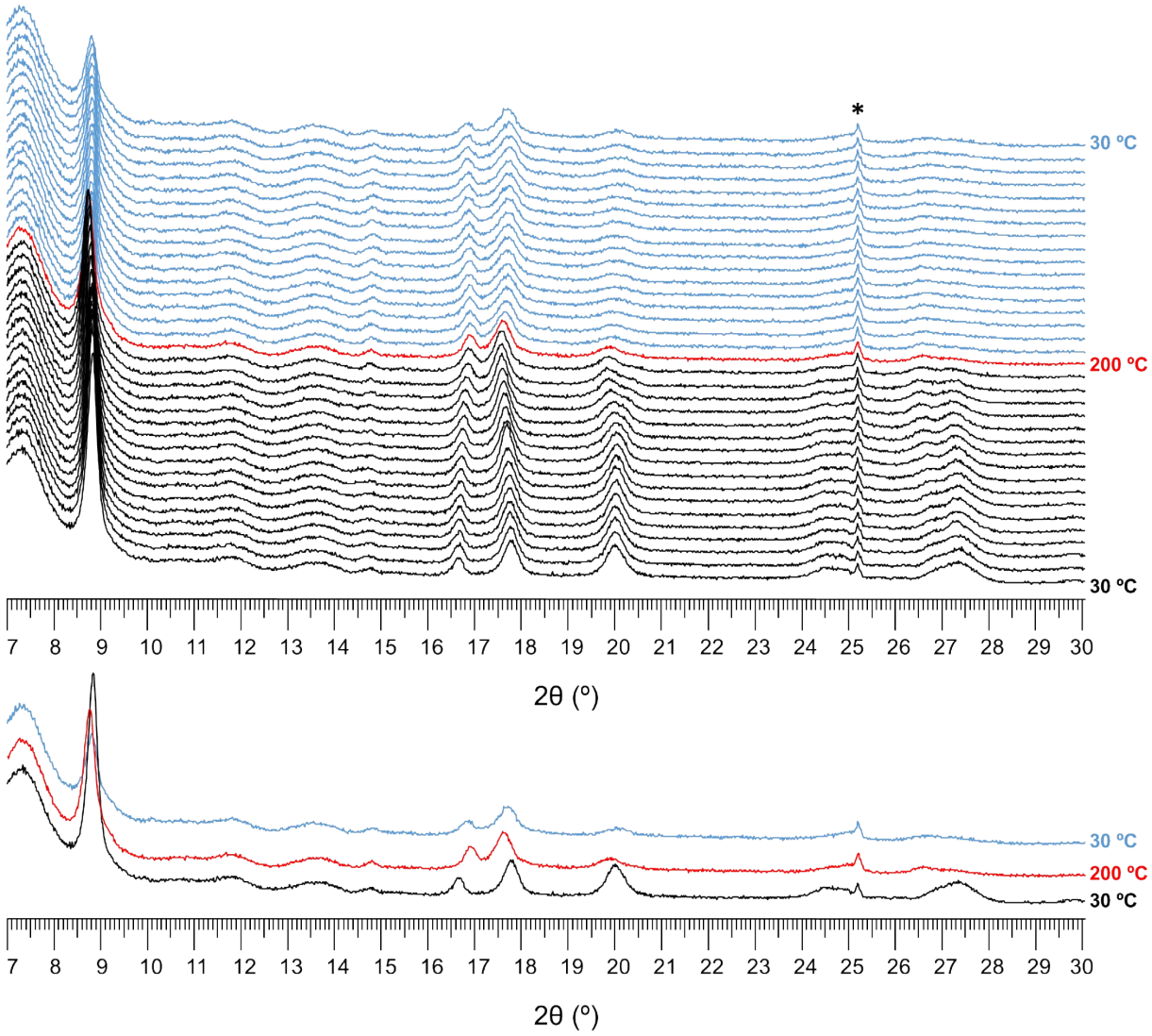

Figure S21: Reversibility VT-PXRD of MIL-47(V)-$(SCH_3)_2 \cdot x CH_3OH$ under air. Comparison of the PXRD patterns at 30 ºC before (black) and after (blue) is shown below. The peak at 25.3 º belongs to the alumina sample holder.

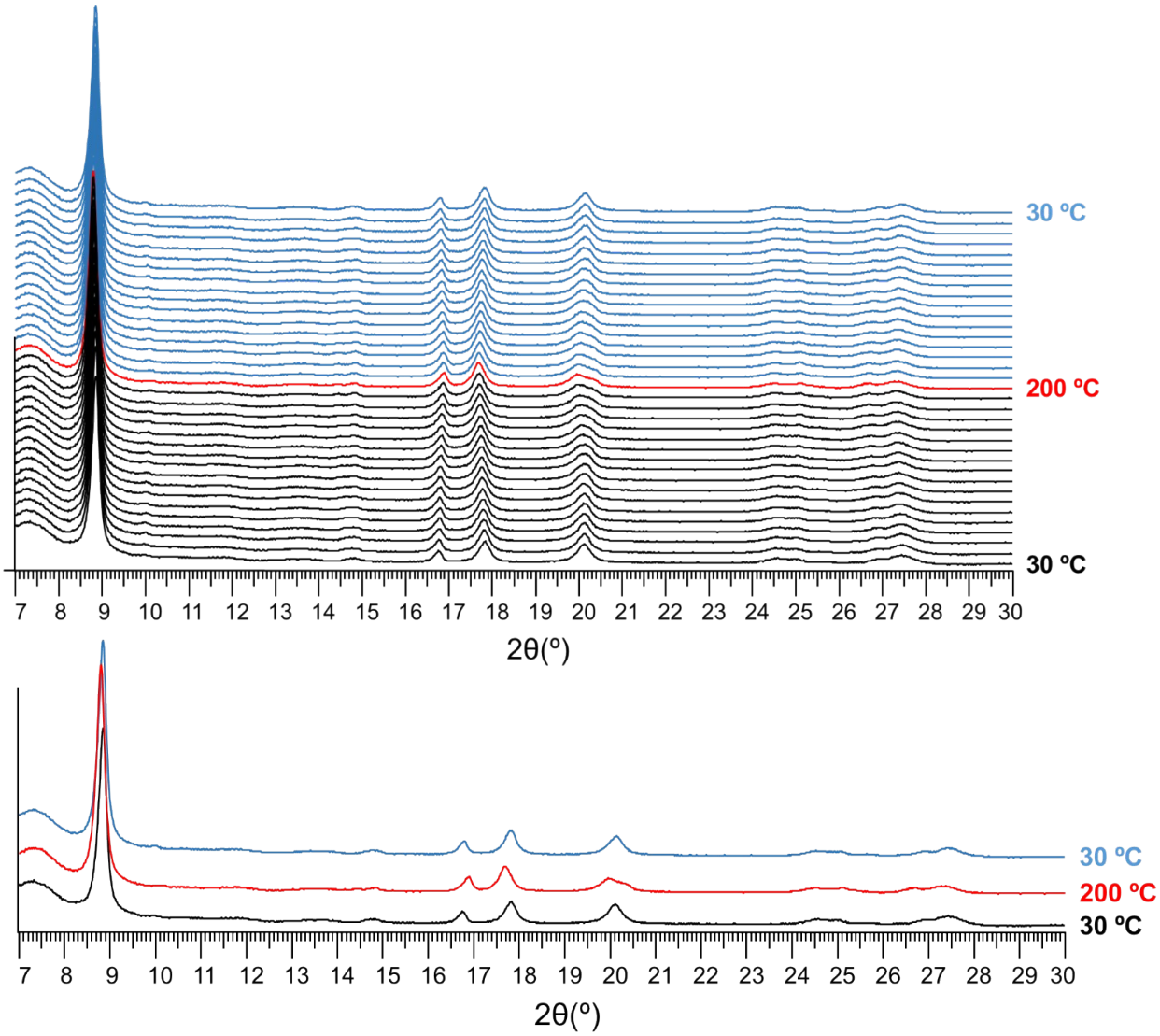

Figure S22: Reversibility VTPXRD of MIL-47(V)-$(SCH_3)_2{\cdot}x CH_3OH$ under N_2. Comparison of the PXRD patterns at 30 ºC before (black), 200 ºC (red) and after (blue) is shown below.

8. Chemical stability

The chemical stability of the material was evaluated by suspending 10 mg of powdered solid in 5 mL of solution (final concentration 2 $mg \cdot mL^{-1}$) under stirring overnight. After, the solids were recovered by filtration ((DMA)KVO(DSBDC)) or centrifugation (MIL-47(V)-$(SCH_3)_2$) and then the PXRD patterns were collected.

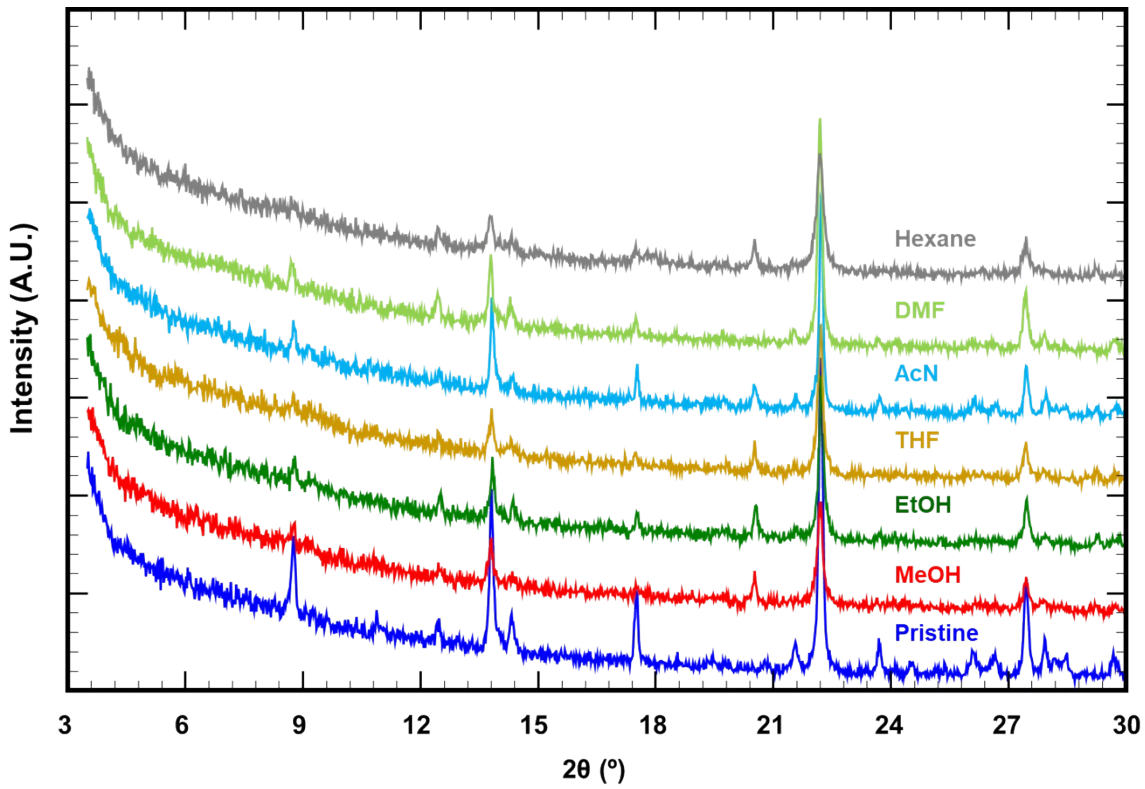

Figure S23: PXRD patterns of the (DMA)KVO(DSBDC) material before and after stability test in different organic solvents.

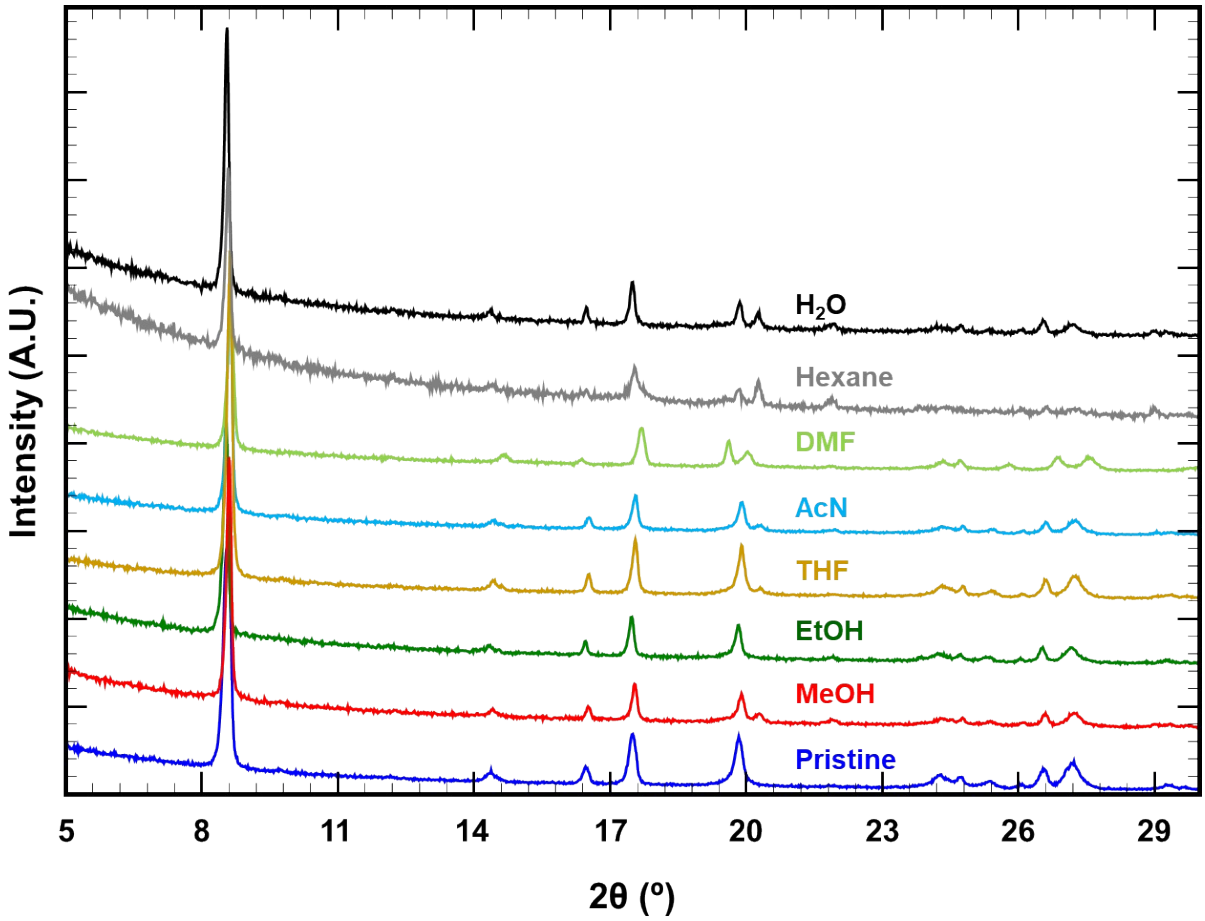

Figure S24: PXRD patterns of the MIL-47(V)-$(SCH_3)_2$·x(MeOH) material before and after stability test in different organic solvents and water.

9. UV-vis spectroscopy

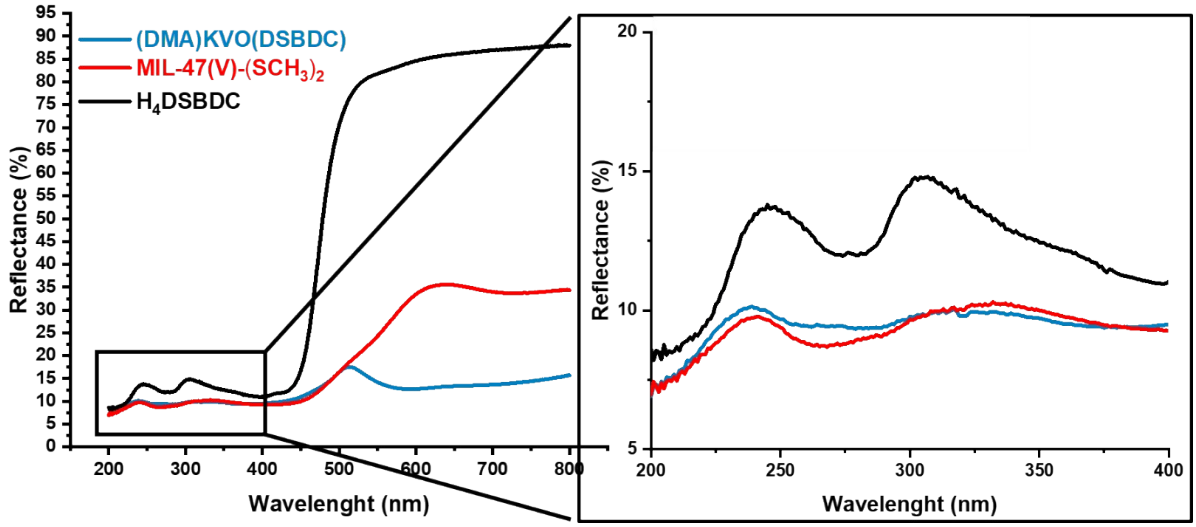

Figure S25: Diffuse reflectance UV-Vis spectra of H_4DSBDC (black), (DMA)KVO(DSBDC) (blue) and MIL-47(V)-$(SCH_3)_2$ (red)

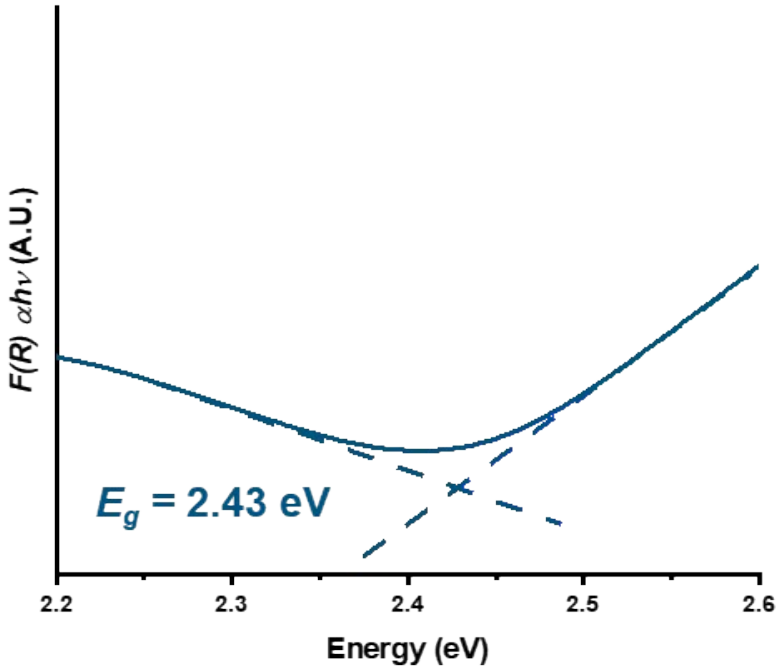

Figure S26. Tauc plot of the (DMA)KVO(DSBDC).

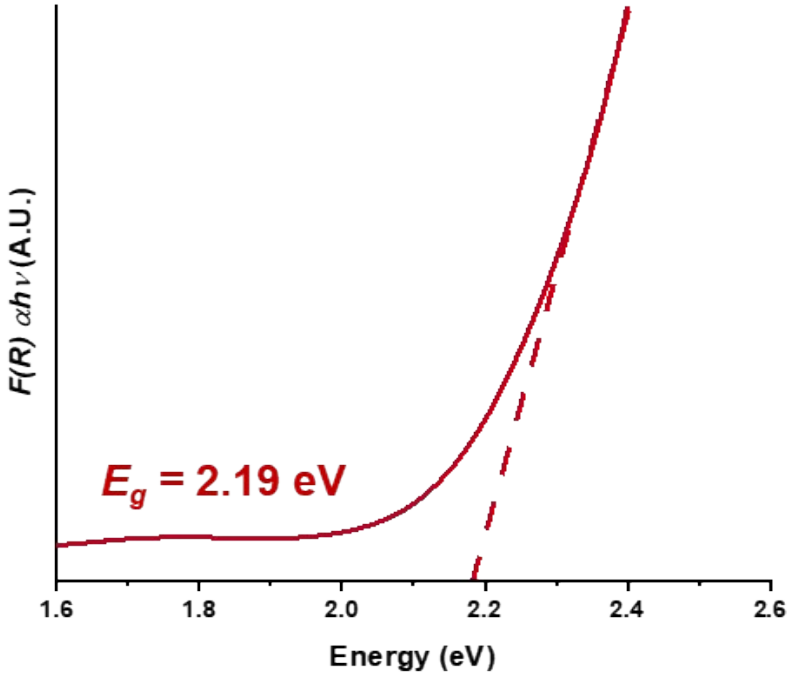

Figure S27. Tauc plot of the MIL-47(V)-$(SCH_3)_2$

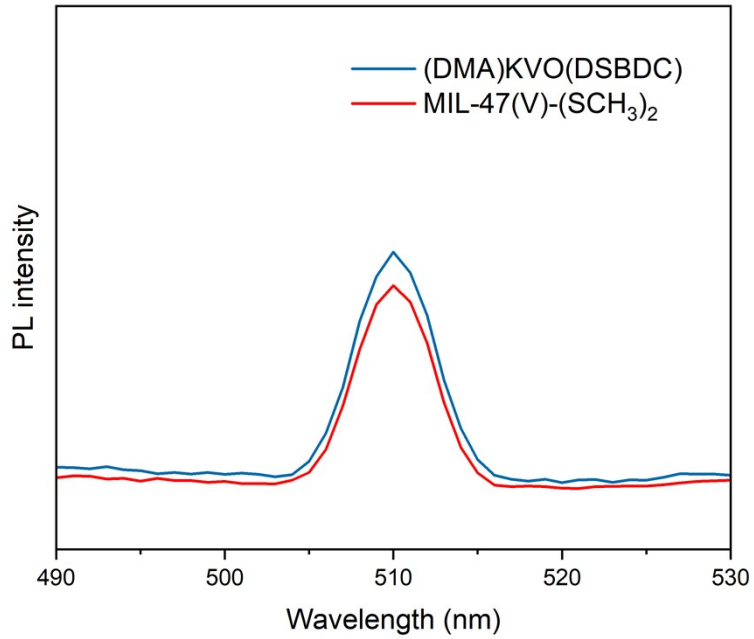

Figure S28: Photoluminescence spectra for (DMA)KVO(DSBDC) (blue) and MIL-47(V)-$(SCH_3)_2$ (red) using an excitation of 415 nm

10. Photocatalytic desulfurization

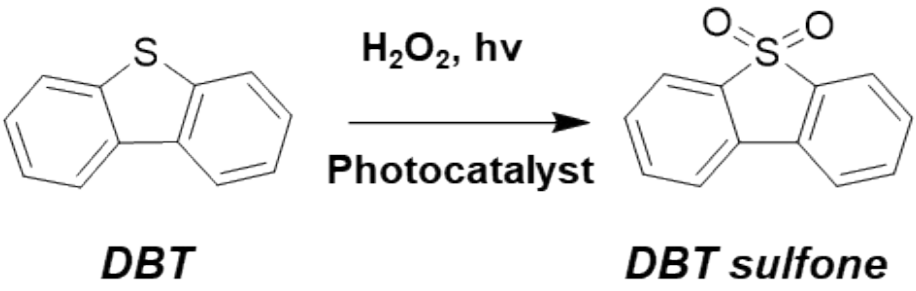

Scheme S1: Photooxidative desulfurization reaction using DBT

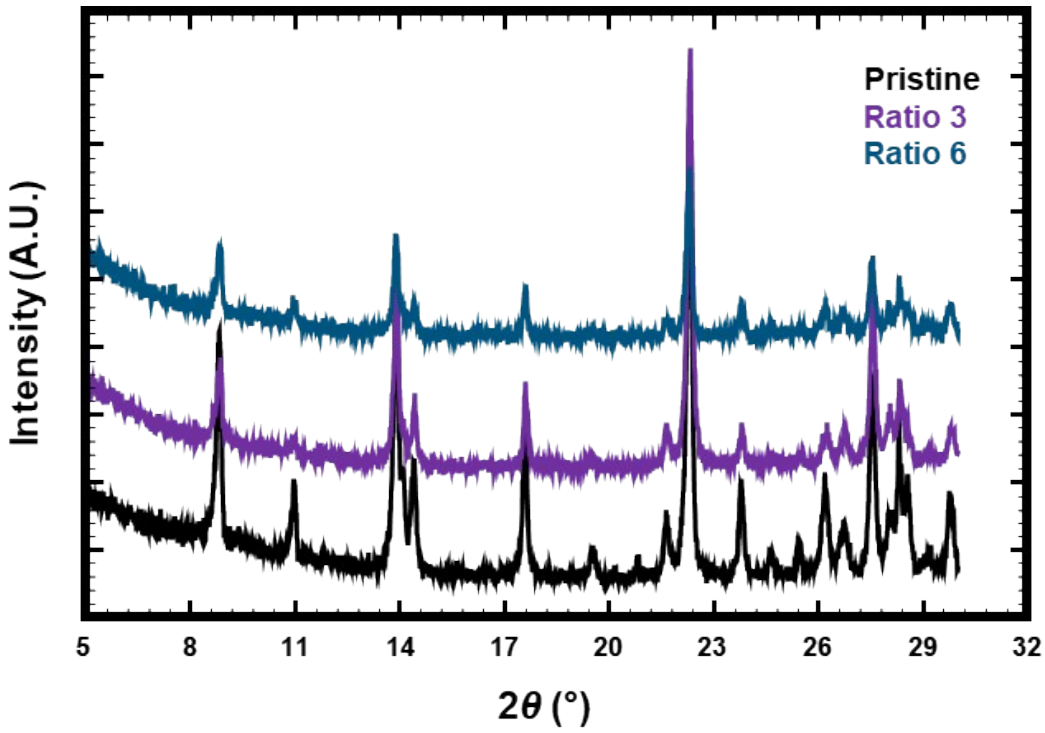

Figure S29: PXRD patterns of the fresh (DMA)KVO(DSBDC) material and after reaction in ACN (ratio 3 and 6)

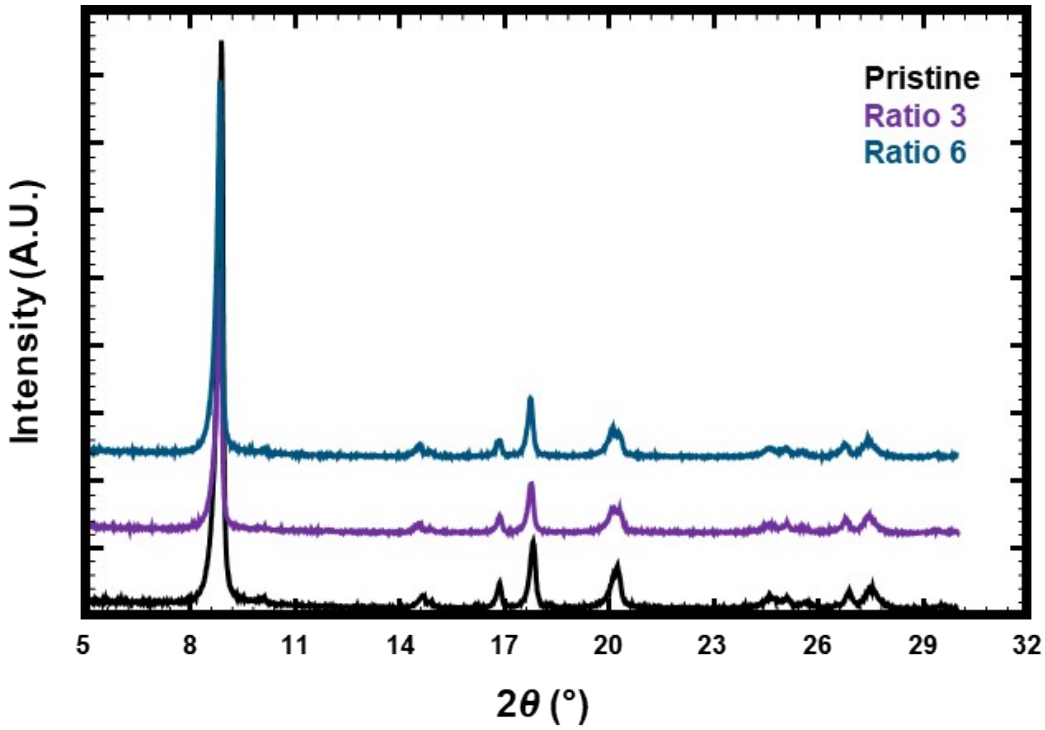

Figure S30: PXRD patterns of the fresh MIL-47(V)-$(SCH_3)_2$ material and after reaction in ACN (ratio 3 and 6)

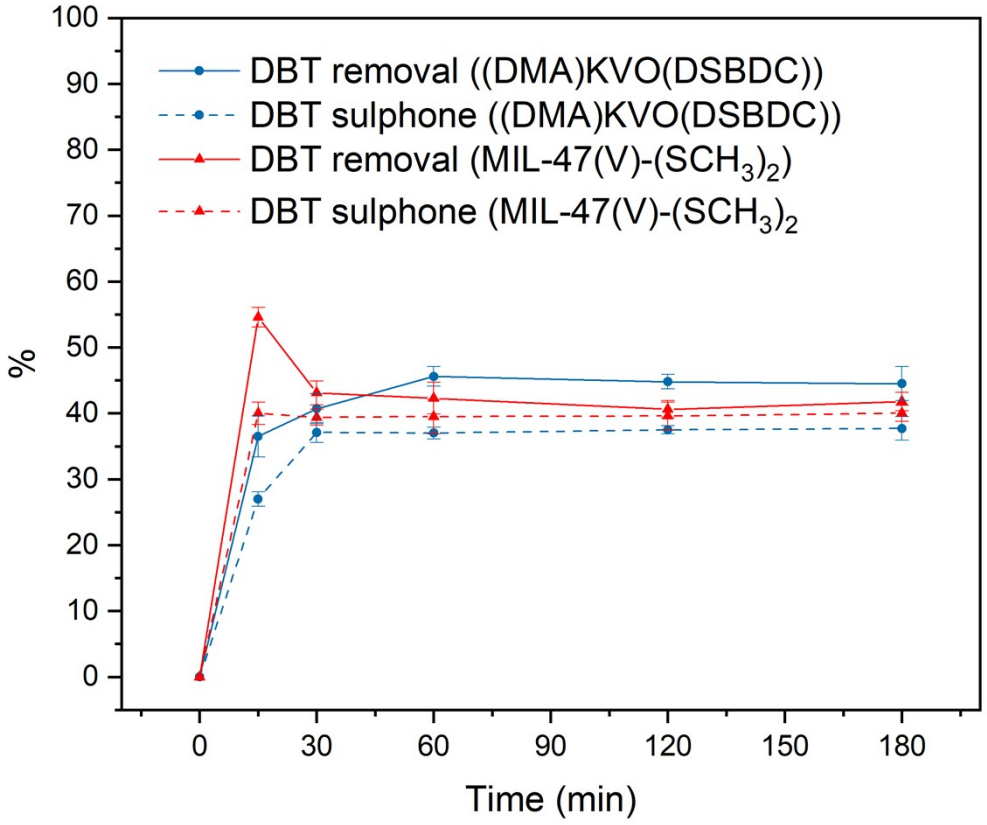

Figure S31: DBT conversion and DBT sulfone using MIL-47(V)-$(SCH_3)_2$ and (DMA)KVO(DSBDC) in liquid-solid phase system (L(ACN)-S(catalyst))

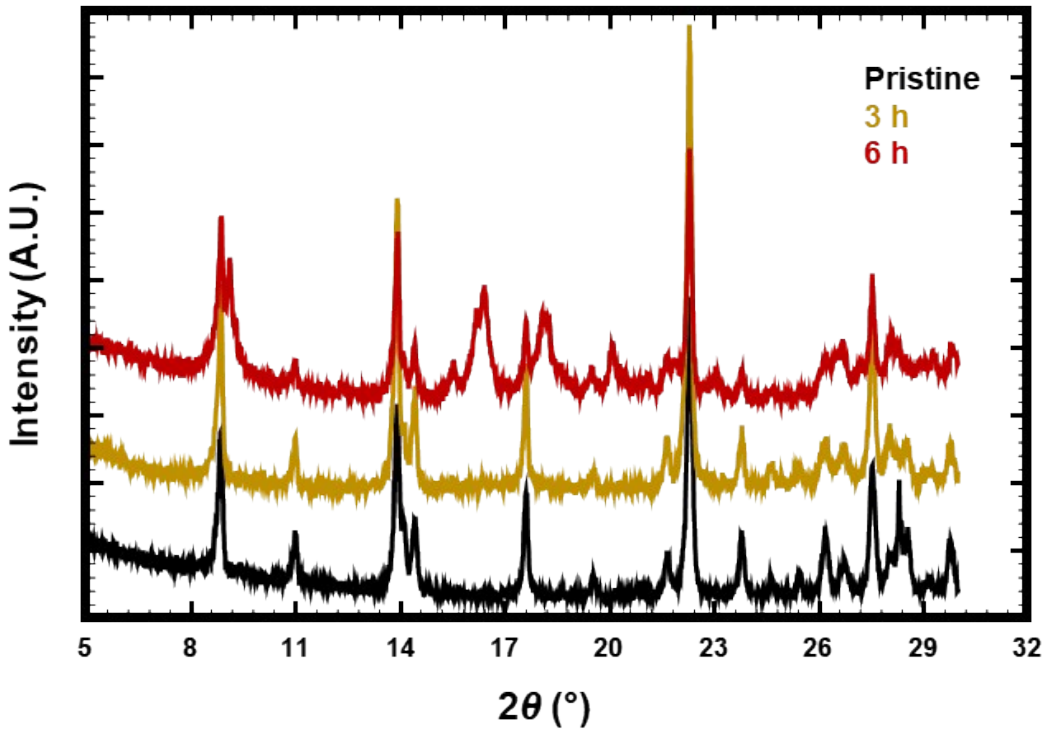

Figure S32: PXRD patterns of the (DMA)KVO(DSBDC) material after 3 h and 6 h reaction time in liquid-liquid-solid phase system (L(ACN)-L(oil)-S(catalyst))

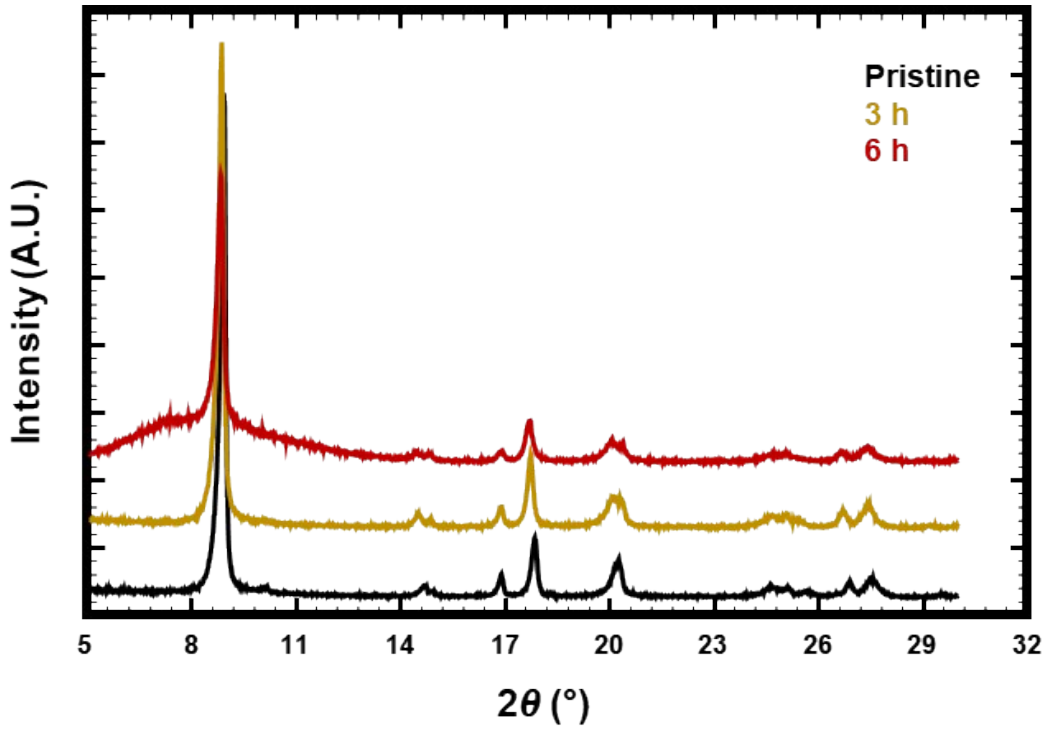

Figure S33: PXRD patterns of the MIL-47(V)-$(SCH_3)_2$ material after 3 h and 6 h reaction time in liquid-liquid-solid phase system (L(ACN)-L(oil)-S(catalyst))

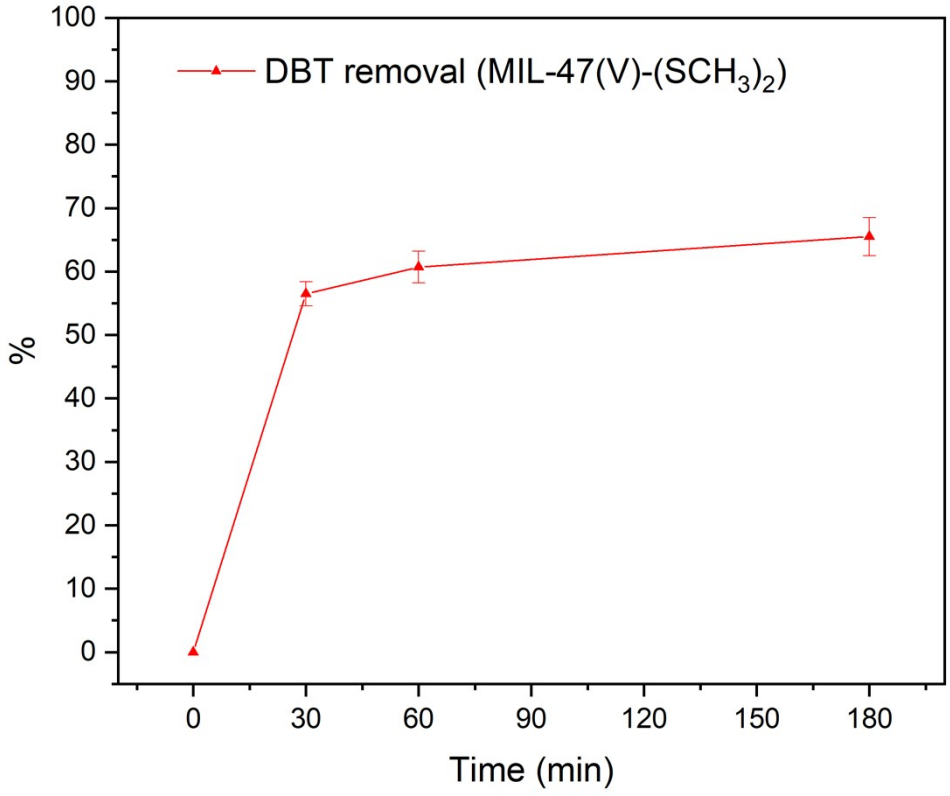

Figure S34: DBT removal using MIL-47(V)-$(SCH_3)_2$ in liquid-liquid-solid phase system (L(ACN)-L(oil)-S(catalyst))

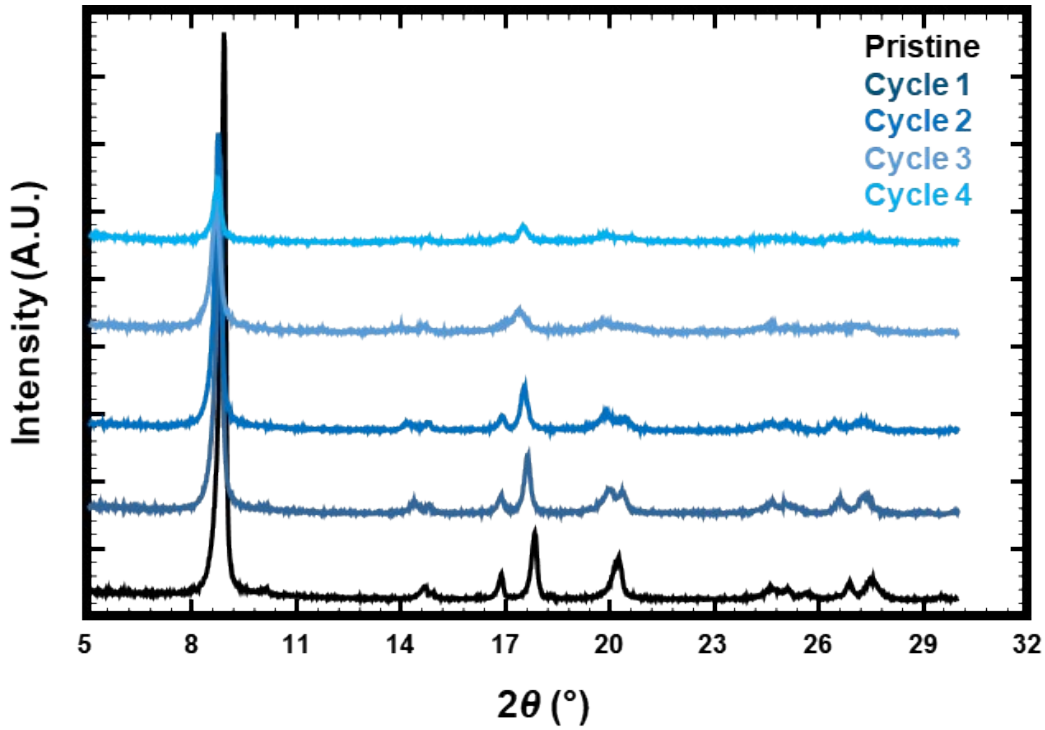

Figure S35: PXRD patterns of the activated MIL-47(V)-$(SCH_3)_2$ and after each 1 h cycle under optimized conditions (H_2O_2 / DBT molar ratio = 12)

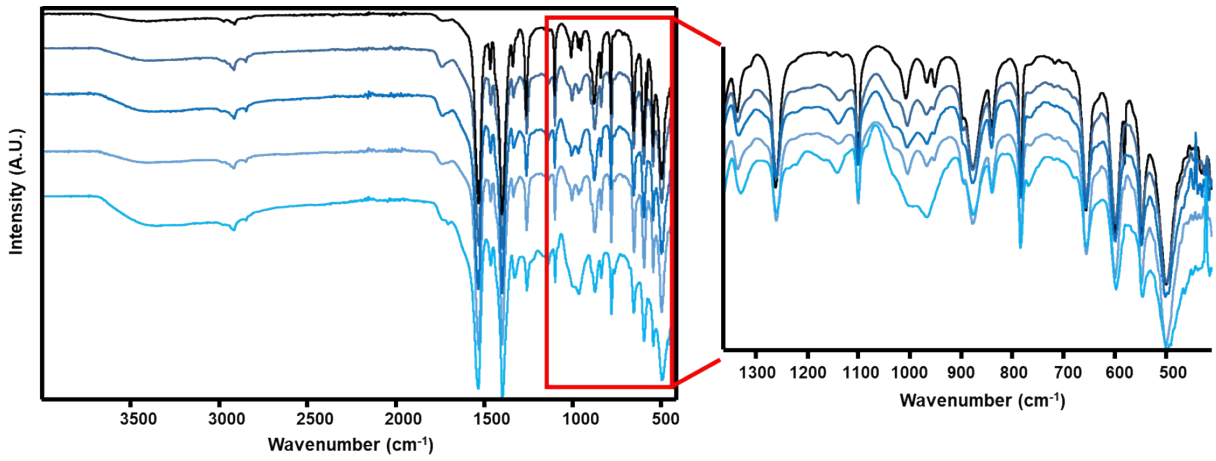

Figure S36: FTIR of the activated MIL-47(V)-$(SCH_3)_2$ and after each 1 h cycle under optimized conditions (H_2O_2 / DBT molar ratio = 12)

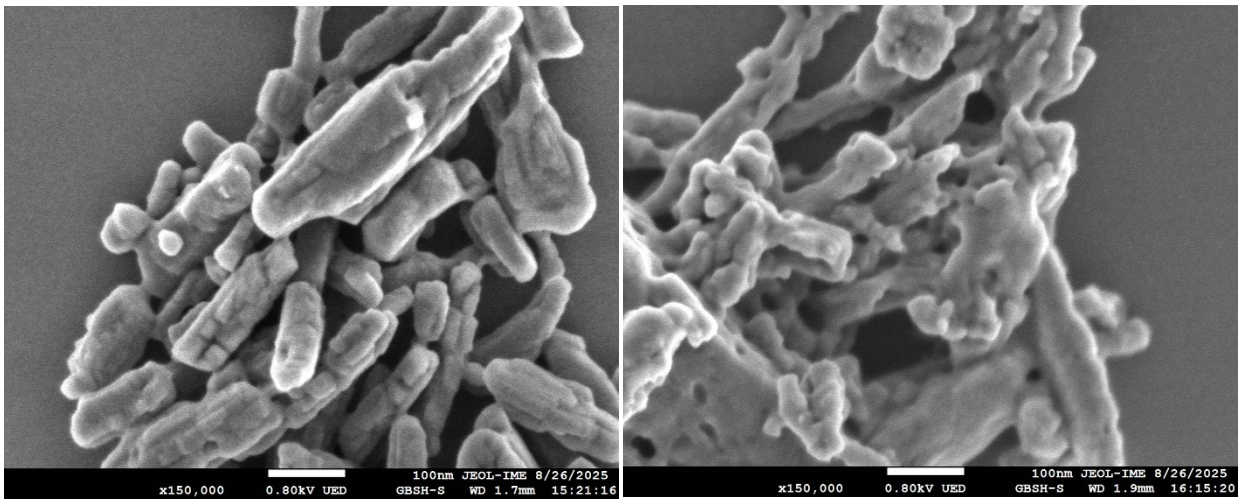

Figure S37: FE-SEM images of fresh MIL-47(V)-$(SCH_3)_2$ (left) and after 4 runs (right)

Table S6. V leeching during the PODS cycling of MIL-47(V)-$(SCH_3)_2$.

Cycle	% V released
1	3.9 ± 0.5
2	5.7 ± 0.2
3	8.1 ± 0.6
4	10.7 ± 0.5